GEOMETRICAL OPTIMIZATION OF A BI-PHASE HYBRID STEPPER MOTOR USING FEM

Ovidiu CRAIU [1*], Teodor Ionuț ICHIM [2]

The paper presents the optimization of a bi-phase hybrid stepper motor (HSM) using a 3D Finite Element Method (FEM) model. The motor is designed for space applications, has a 1° step, and specific outer dimensions. Different shapes of the rotor magnet and stator laminations were modeled to achieve the highest possible holding torque. The ratio between the tooth width and the tooth pitch of the HSM was chosen as 0.4 to maximize holding torque. Single, double, and triple-stack constructions were computed, and the motor's holding torque values were compared.

The 3D FEM model is complex as it includes the motor's refined geometry, such as its very narrow airgap, the end windings, and the surrounding air, which allows computing the magnetic leakage flux.

Keywords: Hybrid stepper motor (HSM), Finite Element Method FEM, holding torque, detent torque, numerical optimization.

1. Introduction

As presented in the literature, the HSM is the synchronous electric machine with the highest torque density. They are robust and have a simple, inexpensive driving system in their most common construction bi-phase motors. In an open loop full-step drive, subsequent pulses are provided on the two phases, with each pulse corresponding to a step movement of the rotor. Most HSMs are constructed with a 1.8° step, but this can also be 1° or even 0.3°, with 50, 90, and 300 teeth on the rotor crown, respectively. More recently, as electronics have developed, the HSMs can now be driven using the well-known field-oriented control (FOC). This ensures more stability of the motor, provides more precision in its movement, and widens the torque-speed characteristic, allowing the HSM to produce more torque at higher speeds when compared to the open-loop drive [1].

The HSM described in this paper operates using an open loop single-step drive with a step of 1°. The motor is designed for a space application with a permanent magnet made of Sm_2Co_{17} (as NdBFe is unsuitable for space

* Corresponding author

[1] Assoc. Prof., Dept. of Electrical Machines, Materials and Drives, Faculty of Electrical Engineering, UNST Politehnica Bucharest, Romania, e-mail: ocraiu@yahoo.com

[2] Assistant Prof. Dept. of Electrical Machines, Materials and Drives, Faculty of Electrical Engineering, UNST Politehnica Bucharest, Romania, e-mail: ichim_teodor@yahoo.com

applications), and a magnetic core made of FeCo laminations in the stator and solid FeCo in the rotor. The stator stack length, the outer and inner diameters are imposed, while the airgap diameter, stator lamination geometry, and magnet size are left to the designer's discretion. The rotor can be built as a single, double, or triple-stack, with each rotor stack consisting of two parallel disk-type rotor-toothed crowns enclosing an axially magnetized permanent magnet in the middle.

Due to its construction, especially its small airgap and toothed rotor crowns, and the presence of both transversal and axial magnetic fields, modeling this motor is challenging. Until recently, researchers used hybrid 2D analytical models to avoid complex and time-consuming 3D modeling [2,3,4]. Even now, there are a limited number of papers studying the HSM, mainly focusing on optimizing the rotor tooth geometry and finding the optimal ratio of tooth width to tooth pitch [5,6,7]. Papers dedicated to the in-depth study of the HSMs using numerical FEM models remain scars [5,8,9,15].

The current HSM was optimized using a 3D FEM model of the magnetic field inside the motor, implemented using the professional software COMSOL Multiphysics v 5.6.

2. Parametrization of the HSM geometry

Due to its physical symmetry (geometrical and sources), only 1/4th of the HSM with a double-stack rotor was studied, which means half of its cross-section and half of its axial length (i.e., one of the two rotor stacks including the end winding on one side of the motor).

The HSM geometry was parametrized based on the data shown in Fig. 1. The HSM external diameter, its inner/shaft diameter, and stator axial length were imposed by the technical specifications as follows: *D_ext* = 69mm, *D_ax* = 41mm, and *l_axial* = 18.6 mm, fig. 2. b).

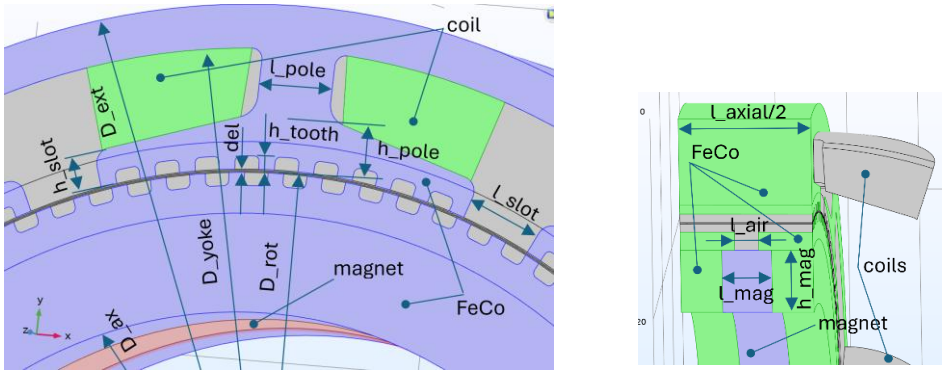

a) b)

Fig. 1. HSM parametrized geometry: a) front view, b) side view.

3. Numerical model

The model was implemented using the professional software COMSOL Multiphysics v 5.6, using the *Rotating Machinery, Magnetic* module [10]. This module allows the user to divide the computational domain into two parts: one representing the stator and the other being the rotor. These parts are "assembled" by connecting the node pairs found on the sliding surface on the stator and rotor subdomains, respectively. This approach eliminates the need to recreate the rotor mesh at each moving step. However, the computational time required for one step of field calculation is larger compared to the "unified" domain where the stator and rotor are directly connected. In this paper, the latter option is considered.

For HSM optimization, only one rotor position was computed: the position of the largest holding torque, which occurs when the stator teeth of the active phase are shifted 1° against the rotor teeth.

The HSM FEM model's discretization is displayed in Fig. 2 without the air surrounding the motor (which is considered in the model but not shown here for clarity). The model includes the geometry of the end winding of the active phase, in yellow in Fig. 2, while the inactive phase is not considered.

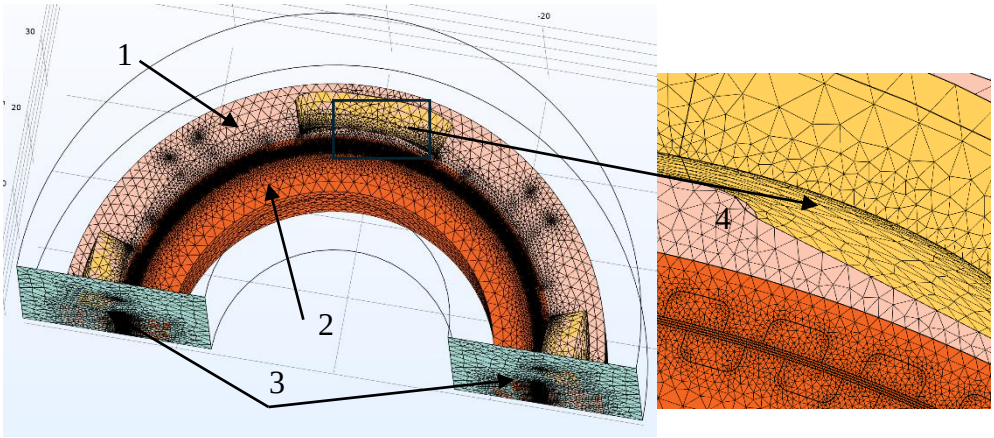

Fig. 2. HSM model discretization: 1 – magnetic vector potential **A** subdomain, 2 magnetic scalar potential V_m domain, 3 – periodic condition surfaces, 4 – discretization mesh detail.

The domain is divided into two regions: one defined by the magnetic vector potential **A** (regions 1 and 4 in Fig. 2) and the other with the magnetic scalar potential V_m (region 3 in Fig. 2), where there are no current sources. The V_m domain was raised from the airgap level (where the **A**-V_m boundary is usually placed according to COMSOL User's Guide recommendation), above the stator teeth (between region 1 and region 2, Fig. 2). Moving a part of the computational domain with fine details (such as the stator teeth) from the vector potential

defined domain under the scalar formulation allowed a significant reduction of the computational time [11].

The electromagnetic torque was computed using Arkkio's relation. This is mathematically equivalent to the virtual work method and provides more precise results than COMSOL's default Maxwellian tensor relation [12]:

$$M = \frac{1}{\mu_0 (r_i - r_e)} \int_{vol} r B_n B_t dv \tag{1}$$

The integration is done over a volume v placed at the airgap level, comprised between an inner radius r_i and an outer (external) radius r_e. B_n and B_t are the normal and tangential components of the magnetic flux density, μ_0 the air magnetic permeability and r the radius.

4. HSM optimization criteria

The optimization of the HSM was based on two criteria: increasing the motor's maximum holding torque at a given terminal voltage and reducing the electrical time constant. A lower electrical time constant allows the current to grow faster when the voltage is applied at the terminals, resulting in the motor producing a greater average torque as the current RMS value per voltage pulse increases.

The conditions for optimization are as follows:

- same rotor axial length and stator stack, rotor inner diameter, and stator outer diameter.
- same airgap dimension del = 0.15 mm for all models.
- phase resistance as close to 55 Ω but not lower.

When comparing coils with the same volume of copper, their resistance and inductance are proportional to the square of the number of turns w^2. When the coil volume changes, the electric time constant becomes proportional to the volume.

In our case, for a constant phase resistance R_{ph}, the winding phase resistance is given by:

$$R_{ph} = \rho \frac{l_{turn} \cdot w \cdot N_{sl}}{S_{co}} = \rho \frac{l_{turn} \cdot w \cdot N_{sl}}{\frac{A_{sl}}{4w} f_{sl}} = \rho \frac{4 l_{turn} \cdot w^2 \cdot N_{sl}}{A_{sl} \cdot f_{sl}} \tag{2}$$

where ρ is the resistivity of copper, l_{turn} is the average length of one coil turn, N_{sl} is the number of slots per phase (in this case $N_{sl} = 4$), A_{sl} is the slot area, and f_{sl} is the filling factor of the slot. As the HSM has redundant windings, one coil occupies $1/4^{th}$ of the slot area. The slot filling factor was considered $f_{sl} = 0.33$.

From eq. (2) it results the number of turns per slot w so that the phase resistance R_{ph} remains constant:

$$w = \sqrt{\frac{R_{ph} \cdot A_{sl} \cdot f_{sl}}{4\rho \cdot l_{turn} \cdot N_{sl}}} = k\sqrt{A_{sl}} \tag{3}$$

All the HSM models computed respect the equation (2). Therefore, any change of the stator lamination geometry that modifies the slot area A_{sl} requires an appropriate modification of the coil turns w.

Based on the relations above, for a given phase current I_{ph} (which is constant for a given terminal voltage and the fixed resistance value of 55 Ω), it yields the ampere-turn in the slot Θ and the equivalent current density J:

$$\Theta = 4 \times w \times I_{ph}, \quad J = \frac{\Theta}{A_{sl}} = \frac{4 \times k\sqrt{A_{sl}} \times I_{ph}}{A_{sl}} = \frac{k'}{\sqrt{A_{sl}}} = \frac{k''}{w} \tag{4}$$

This means the optimization of the current HSM at constant phase resistance, is not performed at constant current density J.

This implies that at a constant phase resistance, the current density inside the slot J will increase as the number of turns w decreases. At the same time, the ampere-turn in the slot Θ and the electric time constant will decrease. Therefore, reducing the HSM number of the coil turns w could be an advantage if the reduction of the ampere-turn in the slot (and thus the torque) could be compensated by an increase in the permanent magnet's contribution to the torque.

5. Numerical results

The FEM models were developed for various geometrical parameters, including a layer of air around the motor to calculate the magnetic leakage flux. Electromagnetic torque was computed for all models considering the rotor shifted with the same 1° from its electrical zero position. Fig. 3 shows the magnetic field density distribution in the middle of the HSM rotor stack, along with the magnetic leakage field lines. The current density vectors inside the numerically computed active coils are shown in red.

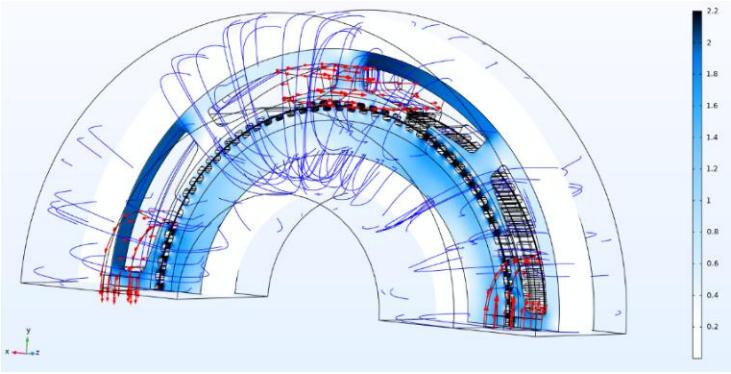

Fig. 3. The magnetic flux density distribution in the HSM middle cross-section (legend units in tesla), the magnetic leakage field lines (blue lines) and the current density vectors (red arrows).

5.1. Modifying the permanent magnet width *l_mag*

The parameter l_{mag} depicting the magnet width, Fig. 1. b), was given three values: 4 mm, 4.5 mm, and 5 mm. Fig. 4 shows the magnetic field distributions in the HSM side sections for the three magnet widths.

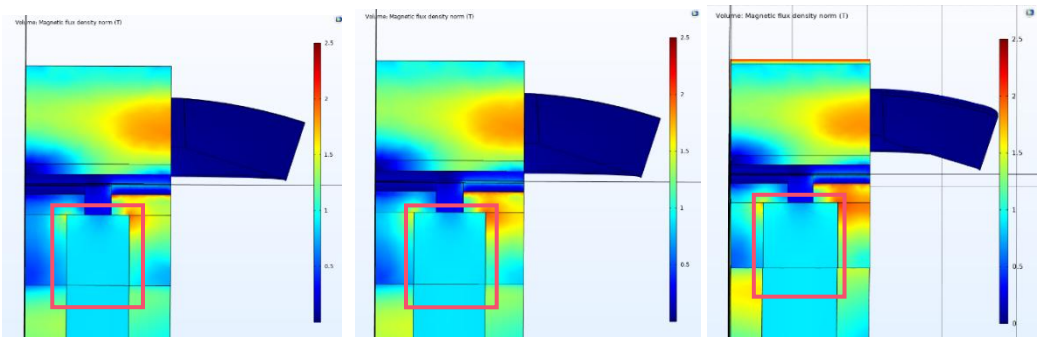

Fig. 4. Magnetic flux density distribution from left to right for (legend units in tesla): *l_mag* = 4 mm, *l_mag* = 4.5 mm and *l_mag* = 5 mm.

Fig. 5 shows that an increase of 25% of the magnet width/volume has generated only a 1% increase in the holding torque. When larger magnets are used, the rotor crowns must be reduced to ensure they all fit within the same axial length. Thinner rotor armatures may lead to higher magnetic saturation (see Fig. 4 on the right).

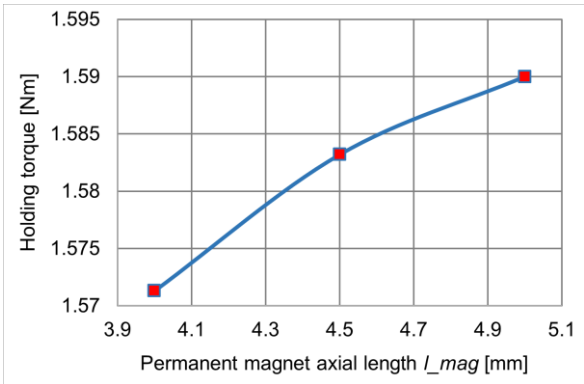

Fig. 5. Holding torque versus magnet width.

5.2. Modifying the permanent magnet height *h_mag*

While in the first study case, the slot area A_{sl} was the same in all models, in this second case, the permanent magnet height was increased along with the outer diameter of the rotor, resulting in a reduced slot area A_{sl}. As the slot area changed, the number of coil turns w had to be adjusted to keep the HSM phase resistance constant. Table 2 lists the number of turns per coil w and the slot area A_{sl} used for the three models.

Table 2

The number of turns per coil w against the slot area A_{sl}.

Permanent magnet height *h_mag*	3.5 mm	4.5 mm	5.5 mm	6 mm
Slot section A_{cr}	92.6 mm^2	75.7 mm^2	56.3 mm^2	47.9 mm^2
Number of turns w	262	235	203	187

Fig. 6 shows the magnetic flux density distributions for different values of the permanent magnet height. As the magnet height increases, the slot area A_{sl} decreases, and so does the coil volume. It is easily observed that the end winding becomes the thinnest for the highest magnet, Fig. 6.d).

Fig. 7 shows that for a 28% increase in the magnet height (also the magnet volume) from 3.5 mm to 4.5 mm, the HSM torque increases by about 15%. At the same time, the number of turns per coil w decreases from 262 turns to 235, which is a positive aspect as that means a lower electrical time constant.

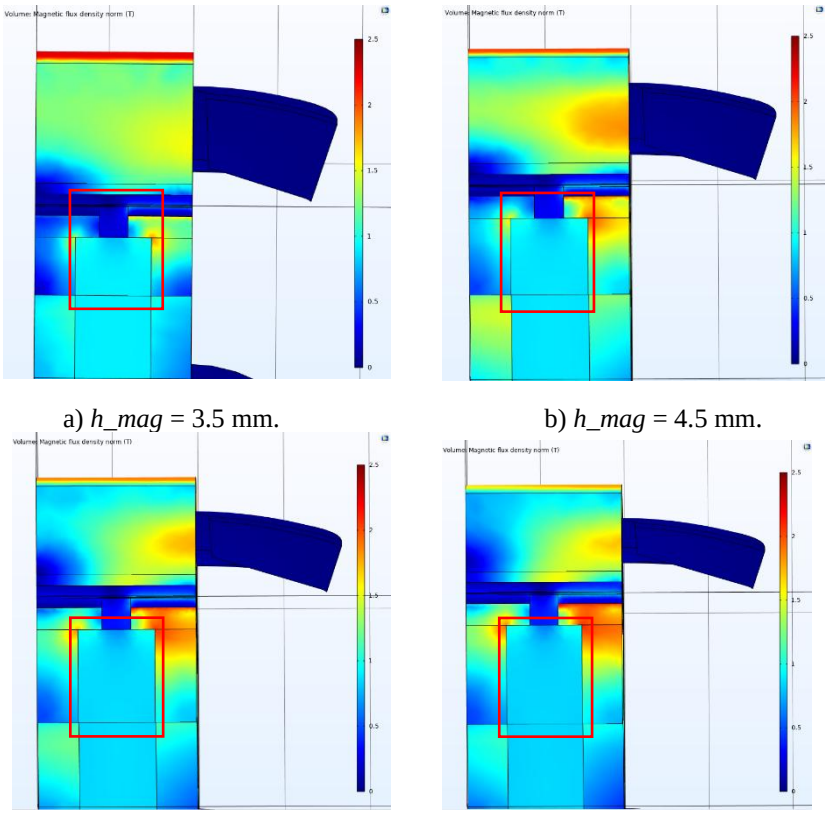

a) *h_mag* = 3.5 mm. b) *h_mag* = 4.5 mm.

c) *h_mag* = 5.5 mm. d) *h_mag* = 6 mm.

Fig. 6. Magnetic flux density distribution (legend units in tesla) for different magnet height *h_mag*.

A permanent magnet with a height above 5.5 mm is not useful as the motor torque diminishes due to a reduced number of ampere-turns.

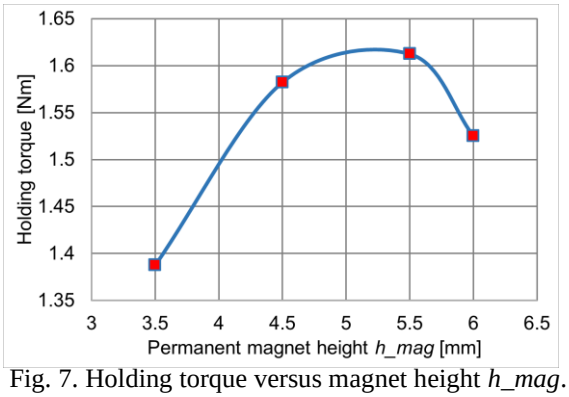

Fig. 7. Holding torque versus magnet height *h_mag*.

A more detailed comparison of the four models using permanent magnets with different heights is presented in Table 3.

Table 3.

Comparison of the HSM having permanent magnets with different heights

Version	Coil turns *w*	Slot area A_{sl}	Magnet height *h_mag*	Copper volume	Stator diameter *D_st*	Phae inductance L	Holding torque
		mm^2	mm	cm^3	mm	mH	Nm
1	262	92.6	3.5	6.1	52	290	1.38
2	235	75.7	4.5	4.9	54	190	1.58
3	203	56.3	5.5	3.6	56	105	1.62
4	187	47.9	6	3	57	74	1.53

5.3. Modifying the airgap between the two rotor disks, *l_air*

The third analysis was about changing the airgap between the two rotor disks, *l_air* in Fig. 1. b). As the airgap was reduced, the surface of the rotor tooth increased, which allowed more magnetic flux to close from the rotor to the stator, Fig. 8. However, when the airgap becomes too small, an increased amount of magnetic flux closes between the two rotor disks, leading to a higher magnetic flux leakage.

The reduction of the *l_air* with 1 mm has a noticeable impact on the torque value, which increased by 7%, Fig. 9. Reducing further the air space between the two rotor crowns diminishes the torque by 8.4 %. This means the ideal distance between the rotor disks is difficult to predict without proper numerical calculation.

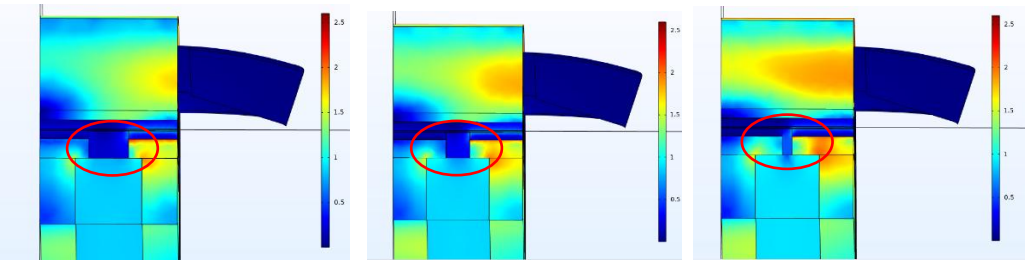

Fig. 8. Magnetic flux density (legend units in tesla) for different values of the airgap between the two rotor disks (from left to right): *l_air* = 0.7 mm; *l_air* = 1.7 mm; *l_air* = 2.7 mm.

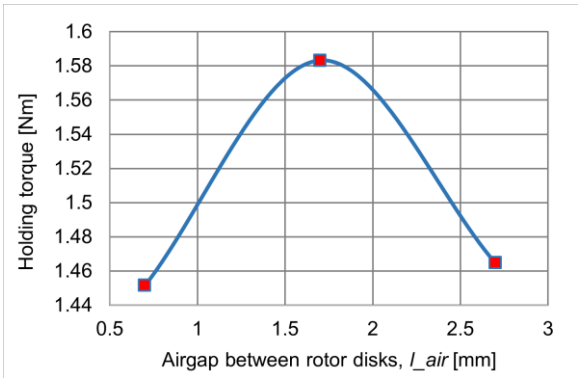

Fig. 9. Holding torque versus airgap length between rotor disks, *l_air*.

5.4. Modifying the height of the stator pole shoe, *h_pole*

Increasing the height of the stator pole shoe allows the reduction of the magnetic saturation in that area. Fig. 10 shows the magnetic flux density distribution in the HSM cross-section for three heights of the stator pole shoe, *h_pole*: 1.5 mm, 1.7 mm, and 1.9 mm. Although the slot area change was reduced, the number of turns per coil had to be modified to respect equation (7): 237, 235, and 232 turns, respectively.

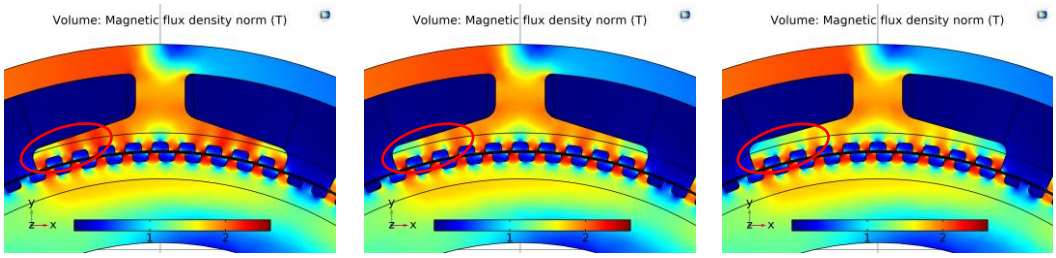

Fig. 10. Magnetic flux distribution for three heights of the pole shoe (left to right,):
h_pole = 1.5 mm; = *h_pole* = 1.7 mm; *h_pole* = 1.9 mm.

The modification of the height of the pole shoe does not seem to have a greater impact on the torque value, Fig. 11. As the height of the shoe pole increased, the slot area decreased and so did the ampere-turns. Thus, despite the reduced magnetic saturation, the HSM configuration with the tallest pole shoe produces a torque reduction of 0.7% compared to the other two solutions.

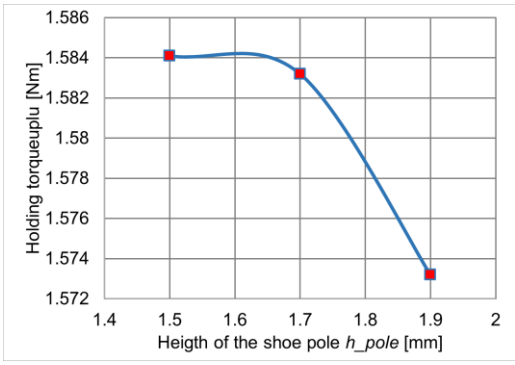

Fig. 11. Holding torque variation against the height of the pole shoe.

5.5. Modifying the stator yoke, *h_yoke*

The last study dealt with the modification of the stator yoke height *h_yoke* (computed as *h_yoke* = (*D_ext* - *D_yoke*)/2, Fig. 1). Reducing the yoke size increased the slot area A_{sl}, which required the adjustment of the turns per coil *w* to respect equation (7). Therefore, for yoke dimensions of 1.5 mm, 2 mm, and 2.5mm, the resulting number of turns per coil *w* were 252, 235, and 271, respectively.

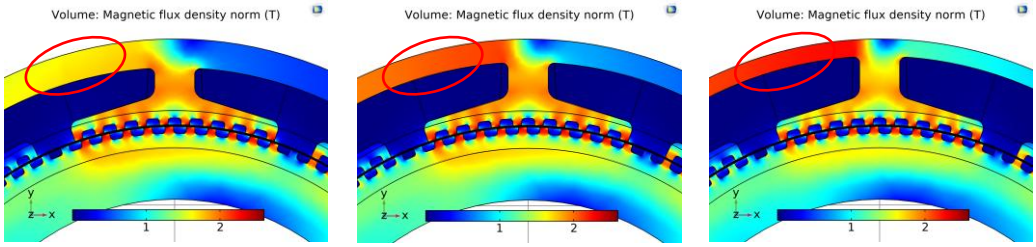

Fig. 12. The magnetic flux density maps for three different yoke dimensions (from left to right), : *h_yoke* = 2.5mm, *h_yoke* = 2 mm, *h_yoke* = 1.5 mm.

A too-narrow yoke of 1.5 mm gets magnetically saturated, Fig. 12, and the torque produced has the lowest value despite the largest slot area and highest number of ampere-turns, Fig. 13. On the opposite side, a too-thick yoke means a lower slot area and reduced ampere-turns, which also means a reduced torque. Compared to the previous geometrical modifications, it appears that the size of the yoke has a stronger effect on the motor's torque. The increase in the yoke size from 1.5 mm to 2 mm has produced a larger torque by about 11%.

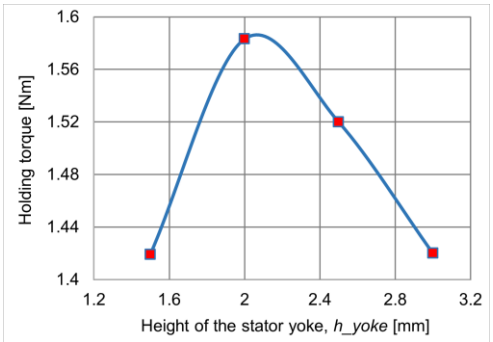

Fig. 13. Holding torque versus the size of the stator yoke.

6. Single, double, and triple rotor stacks

Building HSM with multiple rotor stacks is common. A stack consists of two rotor-toothed disks facing each other and embedding an axially magnetized permanent magnet. Adding more rotor stacks along the axial direction extends the motor length and increases its torque proportionally. As shown further, choosing the right number of stacks is not easy as it depends on the motor geometry, the way the transversal magnetic field closes from one armature to the other, and the permanent magnet geometry. As a rule, the magnet section should not be too far away from a square, also too thin or too thick rotor disks are unsuitable choices, for the motor torque will be reduced.

6.1. The single-stack HSM

Fig. 14 shows an HSM with the same technical requirements as the one presented thus far but in a single-stack construction. Compared to the FEM model of the double-stack motor which consisted of $1/4^{th}$ of the motor, the domain of the single-stack HSM is half of the motor, as there is no axial symmetry.

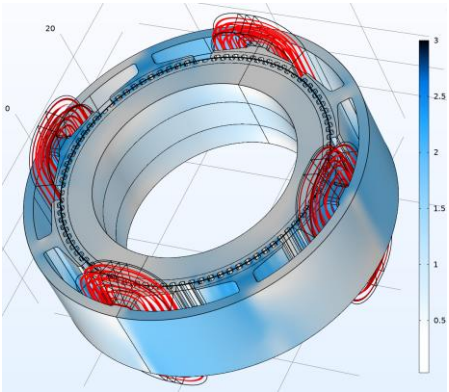

Fig. 14. The single-stack HSM – the magnetic flux density distribution (light blue, legend units in tesla) and current density streamlines (red).

As in the previous simulation, the geometry of the single-stack HSM was optimized. Fig. 15 shows the torque for different stator diameters *D_st* and magnet heights. The same optimization conditions as described in Chapter 4 were used. A smaller diameter is better; however, this means a higher copper volume and an increased electric time constant. The best, compromising solution is the HSM with *D_st* = 56 mm. Still, this motor version produces significantly lower torque than the double-stack version.

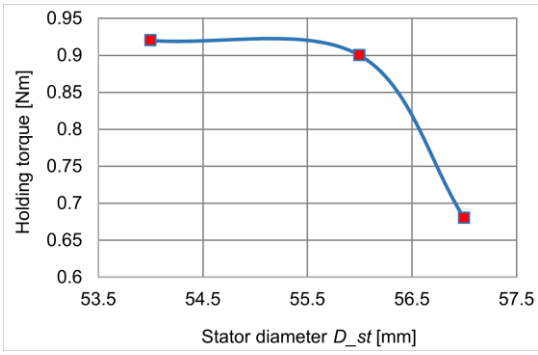

Fig. 15. Holding torque vs stator diameter for single-stack HSM.

6.2. Double stack HSM

This motor has been studied from the perspective of various geometrical parameters, as shown in Chapter 5. The magnet height and the stator yoke have a greater impact on the final HSM torque. Fig. 16 shows the geometry, the magnetic flux density distribution, and the current density streamlines of the motor. Out of the three motors presented in this Chapter, this motor produces the highest holding torque.

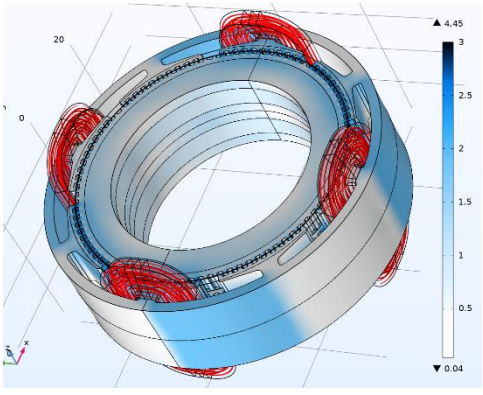

Fig. 16. The double-stack HSM – the magnetic flux density distribution (light blue, legend units in tesla), and current density streamlines (red).

6.3. Triple-stack HSM

Fig. 17 shows the geometry of the triple-stack HSM. As in the single-stack motor, there is no axial symmetry of the motor (due to axially magnetized permanent magnets), which requires modeling half of the motor. The torque values against the stator diameter *D_st* are shown in Fig. 18.

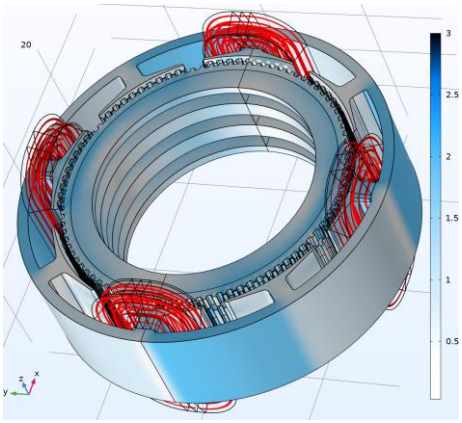

Fig. 17. The triple-stack HSM – the magnetic flux density distribution (light blue, legend units in tesla) and current density streamlines (red).

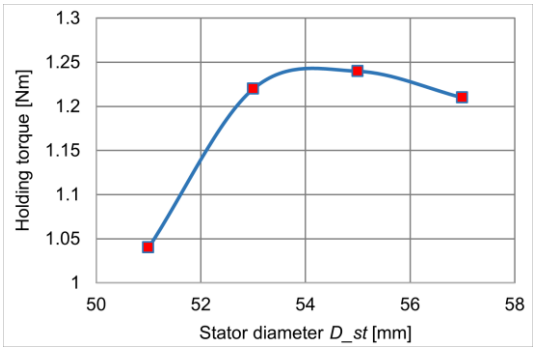

Fig. 18. Holding torque vs stator diameter for single-stack HSM.

7. Conclusions

Designing and sizing an HSM is not easy, mainly because of the intricated combination of its transversal and axial magnetic fields, its very small airgap, and the fact it operates between a saturated and a non/less saturated state (the motor is non-linear). That is why, the only proper models are 3D and must include the leakage flux (the air surrounding the motor), especially the one closing under the rotor permanent magnet. That is different from most motors where leakage flux can be neglected.

The author's goal was to add knowledge regarding the design of a well-known motor and to show some of the important aspects of its optimization. It is clear from the provided results that the HSM design depends not only on the ideal shape of the rotor and stator teeth but also on the geometry of the stator lamination [13,14]. The airgap between the rotor disks, the permanent magnet geometry and the number of stacks are also very important in the motor design.

The HSM presented in this paper was optimized based on several clearly defined criteria. Under different criteria, the results may differ, but the design experience shown here could be useful regardless.

R E F E R E N C E S

[1] *Paul Acarnley*, Stepping Motors a guide to theory and practice 4th edition, The Institution of Engineering and Technology, London, United Kingdom, 2002, Reprinted 2007.

[2] *T. Kosaka and N. Matsui*, "Simple nonlinear magnetic analysis for three-phase hybrid stepping motors," Proc. IEEE Industrial Applications Conf., vol. 1, pp. 126–131, 2000.

[3] *C. Stuebig and B. Ponick*, "Comparison of Calculation Methods for Hybrid Stepping Motors," in *IEEE Trans. on Industry Applications*, vol. 48, no. 6, pp. 2182-2189, Nov.-Dec. 2012.

[4] *Ki-Bong Jang, Seong-Yeop Lim, Tae-Bin Lim, Chang-Sung Jin, Yun-Hyeon Cho, Young-Tae Kim, and Ju Lee*, „2-D FE Analysis of Hybrid Stepping Motor Using Virtual Magnetic Barrier", IEEE Transactions On Magnetics, Vol. 39, NO. 5, SEPTEMBER 2003

[5] *R. P. Praveen, M. H. Ravichandran, V. T. S. Achari, V. P. Jagathy Raj, G. Madhu and G. R. Bindu*, "Design and finite element analysis of hybrid stepper motor for spacecraft applications," 2009 IEEE International Electric Machines and Drives Conference, 2009, pp. 1051-1057.

[6] *I. Ionică, M. Modreanu, A. Morega and C. Boboc*, "Geometry Influence on the Electromagnetic Torque Calculation of a Stepper Motor," *2021 12th International Symposium on Advanced Topics in Electrical Engineering (ATEE)*, 2021, pp. 1-7.

[7] *K. R. Rajagopal, B. Singh and B. P. Singh*, "Optimal tooth-geometry for specific performance requirements of a hybrid stepper motor," in *IEEE Transactions on Magnetics*, vol. 39, no. 5, pp. 3010-3012, Sept. 2003.

[8] *T.I. Ichim, O. Craiu, L.C. Popescu*, "Analyzing a Three Hundred Teeth Bi-Phase Hybrid Stepper Motor with Different Numbers of Pole Pairs", 2023 Rev. Roum. Sci. Techn.– Électrotechn. et Énerg. Vol.68, 3, pp, 283-288.

[9] *O. Craiu, T. I. Ichim, L. M. Melcescu and L. Popescu*, "Optimization of a High Torque Density Small Hybrid Stepper using 3D FEM Model," 2022 International Symposium on Power Electronics, Electrical Drives, Automation and Motion (SPEEDAM), Sorrento, Italy, 2022.

[10] COMSOL Multiphysics, v 5.3, Reference Manual, User's Guide, Copyright© 1998-2018.

[11] *O. Craiu, T. -I. Ichim and L. C. Popescu*, "3D FEM Model of a Hybrid Stepper Using Scalar-Vector Potential Formulations," 2023 13th International Symposium on Advanced Topics in Electrical Engineering (ATEE), Bucharest, Romania, 2023, pp. 1-5.

[12] *Arkkio*, Analysis of Induction Motors Based on the Numerical Solution of the Magnetic Field and Circuit Equations, PhD Thesis, Helsinki 1987.

[13] *L. Mariolo, Lucia Frosini, A. Rubino, D. Spelta*, „ Modeling of Hybrid Stepper Motor Finalized to the Optimization of the Holding Torque", 2021 IEEE Workshop on Electrical Machines Design, Control and Diagnosis (WEMDCD).

[14] *M. Onsal, M. Aydin, Y. Demir, M.K Guven*, „Impact of Airgap on the Performance of 3-Phase Permanent Magnet Hybrid Stepper Motor", IECON 2021 - 47th Annual Conference of the IEEE Industrial Electronics Society.

[15] *A. I. Chirila, I. -D. Deaconu, V. Navrapescu, M. Albu and C. Ghita*, "On the model of a Hybrid Step Motor," 2008 IEEE International Symposium on Industrial Electronics, Cambridge, UK, 2008, pp. 496-501.